ACS APPLIED MATERIALS & INTERFACES

Research Article

www.acsami.org

Improved Polymer Encapsulation on Multiwalled Carbon Nanotubes by Selective Plasma Induced Controlled Polymer Grafting

Sunanda Roy,[†] Tanya Das,[‡] C. Y. Yue,*[,‡] and Xiao Hu*[,†]

[†]School of Materials Science and Engineering, Nanyang Technological University, Singapore 639798

[‡]Singapore−MIT Alliance, Manufacturing Systems and Technology Programme, School of Mechanical and Aerospace Engineering, Nanyang Technological University, Singapore 639798

ABSTRACT: Surface graft polymerization on multiwalled carbon nanotubes (MWCNTs) with several grafting mechanisms is nowadays a demanding field of nanocomposites in order to enhance the load carrying capacity, thus improving the overall performance of the composites. Here, we demonstrate the covalent grafting of a sulfonic acid terminated monomer, 2-acrylamido-2-methylpropane sulfonic acid onto sidewalls of MWCNTs via a comparative study between oxygen plasma induced grafting (OPIG), nitrogen plasma induced grafting (NPIG), and nitrogen + oxygen plasma induced grafting (NOPIG) with the aim to identify the most effective process for the preparation of polymer encapsulated carbon nanotubes. From the detail surface analysis, it has been noticed that NOPIG offered much better surface grafting than that of the OPIG and NPIG. The transmission electron microscopy (TEM) images showed that MWCNTs modified by NOPIG possess much thicker and uniform polymer coatings throughout. From thermogravimetric analysis (TGA), the grafting degree was found to be ∼80 wt % for the NOPIG sample.

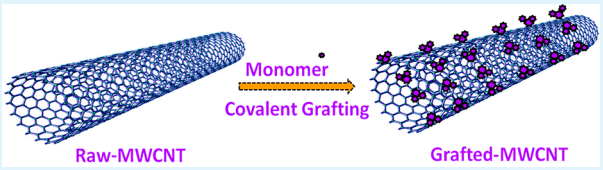

KEYWORDS: *covalent grafting, dispersion, tensile strength, aggregations*

INTRODUCTION

Since first reported by Iijima in 1991,[1] carbon nanotubes (CNTs) have received immense scientific and technological interest in a wide range of applications such as photovoltaic devices,[2,3] superconductors,[4] gas storage media,[5] lithium batteries,[6,7] electromechanical capacitors,[8] high performance polymer composites,[9−14] biomaterials, and drug delivery vehicles,[15,16] owing to their excellent intrinsic properties such as high elastic modulus, high tensile strength, good elongation at break, large aspect ratio, high thermal stability, and excellent conductivity. Despite the above mentioned advantages, in most of the cases it has been noticed that the raw CNT surfaces were subjected to undergo various modification with different functional groups before being considered. The explanation behind this is to reduce the tendency of formation of agglomeration due to high surface energy, high aspect ratio, and strong van der Waals force in raw CNTs, which hinders homogenous dispersion of the same in a polymer matrix. Moreover, the raw CNTs are insoluble in most commonly used organic solvents due to their hydrophobic, nonreactive surface properties. Therefore, surface functionalization of CNTs has been extensively studied to tailor the physical properties of CNTs and hence, to improve the interactions between CNTs and polymer matrices, or solvents and thus expand their application into more advanced fields. In this regard, several strategies including acid treatment, fluorination, polymer wrapping, mechano-chemical treatment, and plasma treatment have been studied.[17−22] Among those, the acid treatment process has gained much attention as it facilitates the chemical reactivity of the graphene structure by carboxylic acid functionalisation as well as purifies the CNT structure. These acid groups can exfoliate the CNT bundles, thus improving the solubility in polar medium. However, this acid treatment causes severe damage to the tip and sidewalls of the nanotubes, and can even break the CNTs into shorter tubes[23] due to the vigorous reaction pattern. As a result, the acid treated nanotubes exhibit significant loss in conductivity and reinforcing capabilities. Moreover, it produces huge amounts of acid wastes that are environmentally hazardous.

In recent years, a great deal of research has been devoted to the surface modification of CNTs by plasma treatment,[24−27] although it was invented mainly for the purpose of polymer surface modification to improve the polymer surface hydrophilicity, biocompatibility, and adhesion strength. The reasons behind using the plasma treatment are such that it is a simple, fast, uniform, and environmentally safe process, as no hazardous chemical is utilized. Using this process, a wide range of functional groups can be inserted to the CNTs by variation of the process gas and plasma parameters, which in turn can act as active sites for further functionalization by other molecules. The major advantage of plasma treatment is that it only modifies the surface properties of the nanotubes without affecting the bulk properties. Therefore, plasma functionalization induces less damage to the structure of the nanotubes as compared to the acid treatments. Some previous studies have shown that polymer coated CNTs exhibited much higher stable

Received: October 28, 2013
Accepted: November 5, 2013
Published: November 5, 2013

aqueous dispersion than the direct introduction of the functional groups on it.[28,29] On the basis of this fact, lots of methodologies such as acid treated grafting,[30,31] chemical grafting,[32,33] radiation induced grafting,[34] atom transfer radical polymerization (ATRP),[35] living anionic polymerization,[36] and ring-opening polymerization[37] have been employed in last few years for covalent grafting of hydrophilic monomers on the surface of CNTs. However, currently the green chemistry techniques have earned great interest to modify surfaces under eco-friendly, safe, and mild conditions with low energy consumption. In this regard, plasma induced grafting has become a major interest of research to modify the CNT surfaces by fast, safe, low cost, and more controllable ways.

Therefore, in the current communication, we present three facile methodologies for the graft polymerization of hydrophilic monomer onto the pristine MWCNTs by means of oxygen plasma induced grafting (OPIG), nitrogen plasma induced grafting (NPIG), and nitrogen + oxygen plasma induced grafting (NOPIG) to identify the most effective grafting process. The radio frequency plasma process was used as it is a versatile process for the surface treatment of polymers. The 2-acrylamido-2-methylpropane sulfonic acid (AMPS) monomer has been chosen for the grafting as it is hydrophilic, biocompatible, and water-soluble. Moreover, due to the presence of $-SO_3H$ group in AMPS, we hypothesize that polyAMPS grafted MWCNTs (PAMPS-*g*-MWCNTs) can be used in a wide range of applications including humidity sensors, chemical sensors, proton exchange membranes, drug delivery, and bio-nanocomposites.

EXPERIMENTAL METHODS

Materials and Reagents. MWCNTs with an outer diameter of less than 8 nm, a length of 10−30 μm, and a purity over 95% were purchased from Cheap Tubes and used as received. The monomer, acrylamido-2-methylpropane sulfonic acid (AMPS, 99% purity), and solvents such as acetone, methanol, toluene, and *N*,*N*-dimethyl formamide (DMF, 99.8%) were all purchased from Sigma Aldrich, Singapore (ACS grade).

Plasma Treatment of MWCNTs. The plasma excitations of MWCNTs were performed using a low pressure plasma source with a radio frequency (rf) of 13.56 MHz. The plasma chamber contains four separate aluminum shelves where the samples to be treated were kept. The system was equipped with two mass flow controllers (MFCs). Prior to plasma treatment, raw MWCNTs were pretreated by dispersing it into DMF solution and irradiated with a 20 kHz ultraprobe sonicator for 10 min. After the solution was vacuum dried (12 h), the MWCNTs were subjected to the oxygen (O_2-MWCNTs), nitrogen (N_2-MWCNTs), and nitrogen + oxygen plasma (N_2+O_2-MWCNTs) treatments. This was done to separate the nanotubes from their intrinsic large aggregations by destroying the van der Walls forces. For each plasma treatment, ∼60 mg of MWCNTs was separately exposed to the O_2, N_2, and N_2 + O_2 plasmas for 5 min at a plasma power of 300 W. For O_2 and N_2 plasmas, the flow rate was set to 75 sccm and for the N_2 + O_2 plasma it was 50 and 25 sccm, respectively. After the plasma treatments, the treated MWCNTs were air exposed for 30 min.

Preparation of Plasma Induced Grafting (PAMPS-*g*-MWCNTs). For the preparation of plasma induced grafting sample, the three plasma treated CNTs were transferred into three separate round bottom flasks containing the monomer solution (20 wt %) and were degassed by continuous nitrogen bubbling with constant stirring. The graft polymerization was performed by heating the mixture for 8 h under continuous stirring at 70 °C. Next, the grafted MWCNTs were thoroughly washed by deionized water and acetone mixture to remove the homopolymer and unreacted residuals. Then, the purified PAMPS-*g*-MWCNTs were dried in vacuum oven at 80 °C overnight and stored in small glass bottles with proper labeling.

Characterizations. The chemical compositions of the raw, plasma treated, and monomer grafted MWCNTs were determined using a Perkin-Elmer GX Fourier transform infrared spectroscope (FTIR) in transmission mode using potassium bromide (KBr) pellets at 32 scans and resolution of 4 cm^{-1}.

X-ray photoelectron spectroscopy (XPS) with monochromatic Al Kα as an X-ray excitation source operating at 15 kV and 10 mA was used to determine the elemental compositions on the CNT surfaces. A step-scan interval of 1 eV was used for wide scans, and 0.1 eV for high resolution scans; the acquisition times were 60 s for both resolutions. Binding energies were referenced to the saturated hydrocarbon peak at 285 eV.

Raman spectroscopy was carried out on a WITec CRM200 Confocal Raman microscope (488 nm laser) to investigate the structural changes of MWCNTs.

Thermogravimetric analysis (TGA) was conducted using a Perkin-Elmer TA Q500 instrument from 30 to 800 °C at a heating rate of 10 °C min^{-1} under nitrogen gas flow.

Transmission electron microscopy (TEM) observations were performed on a JEM-2100F electron microscope.

The dispersion stability of raw and all the modified CNTs were determined by dispersion of nanotube powders in methanol using an ultrasonic bath for 1 h. In each case, 25 mg of CNTs was added into 5 mL of methanol. Then, the MWCNTs/methanol solutions were left to stand at room temperature and images were captured at fixed time intervals.

RESULTS AND DISCUSSION

It is well-accepted that plasma methods are quite complex, and the mechanism is still ambiguous.[38] However, some literature has shown that, during plasma treatment, numerous active radicals are generated on the polymer surfaces depending on the reactive gas flow.[38,39] Later, most of these radicals were converted into peroxide, hydroperoxides, and other active species in the presence of oxygen in the plasma or the exposure of air after plasma treatment in inert gases such as argon and nitrogen. These peroxide radicals that formed are believed to be stable at room temperature.[28] These peroxides, in presence of heat, decompose into free active radicals that initiate the polymerization of various monomers such as vinyl, acryl, and also result in cross-linking of polymer coatings.

The evidence of polymer grafting onto the surface of the MWCNTs was confirmed by comparing the FTIR spectra of the raw, AMPS, and three differently modified MWCNT samples (Figure 1). It can be seen from Figure 1a that the raw MWCNTs exhibited two weak absorption peaks at 1588 and 3444 cm^{-1} due to C═C and OH groups,[30,33] respectively. The presence of the hydroxyl (−OH) group in the raw MWCNTs could be assumed to be the results of mild surface oxidation during the purification when manufactured. Compared with the raw MWCNTs, the polymer grafted MWCNTs (PAMPS-*g*-MWCNTs) showed (Figure 1b−d) some new and distinctive peaks within the same wavenumber region. For any PAMPS-*g*-MWCNTs, the broad absorption band at 3440 cm^{-1} was due to the overlapped band of −NH and −OH stretching vibrations. The characteristic peaks at 1667 and 1553 cm^{-1} were assigned to the C═O stretching (amide I band) and N—H bending (amide II band),[40] respectively. In addition, the new peaks at around 1372 and 1028 cm^{-1} were attributed to the characteristic stretching vibrations of the $-SO_3$ group.[41] The peaks present at 3039 and 2986 cm^{-1} corresponded to the C—H stretching frequency of $-CH_3$ and $-CH_2$ bonds. It is also apparent from Figure 1b−d that among the three grafted

dx.doi.org/10.1021/am404768v | ACS Appl. Mater. Interfaces 2014, 6, 664−670

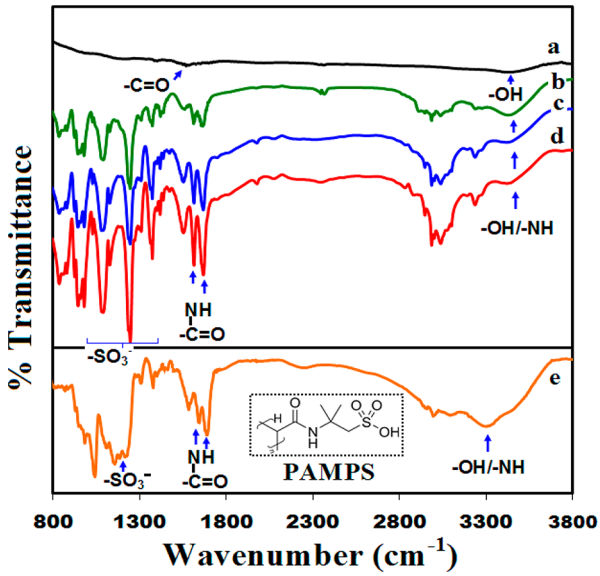

Figure 1. ATR-FTIR spectra of (a) raw MWCNTs, (b) NPIG-PAMPS-*g*-MWCNTs, (c) OPIG-PAMPS-*g*-MWCNTs, (d) NOPIG-PAMPS-*g*-MWCNTs, and (e) PAMPS.

MWCNTs samples, NOPIG-PAMPS-*g*-MWCNTs (Figure 1d) had the highest FTIR peak intensities for the carbonyl, amide, and SO_3 groups. Because the intensity of the peak increases with increasing the grafting yield/degree, it can be assumed that NOPIG is the more effective surface grafting technique than that of OPIG and NPIG.

Figure 2 shows the Raman spectra of the raw MWCNTs (Figure 2a), O_2-MWCNTs (Figure 2b), N_2-MWCNTs (Figure 2c), N_2+O_2-MWCNTs (Figure 2d), and three different PAMPS-*g*-MWCNTs (Figure 2e–g). As can be seen, there are three distinct peaks in all spectra. The peaks appeared at approximately 1351 and 1576 cm^{-1} denoted as the D and G bands,[26,28] respectively. The D band is assigned to the A_{1g} breathing mode. This mode is generally attributed to the defects in the curved graphite sheet, sp^3 carbon (C—C), amorphous carbon, or other impurities.[42] The G band is associated with the E_{2g} in-plane stretching vibration mode in the basal plane of graphite, which indicates the presence of crystalline graphitic carbon (C═C) in CNTs samples.[28] Another characteristic peak at the higher frequency side of 2677 cm^{-1} is the second harmonic of the D band, referred to as D*, and is independent of the defect concentration. The ratio of intensity of the D and G bands, (I_D/I_G), was calculated to determine the relative extent of structural defects in the MWCNTs due to surface modification. In the raw MWCNTs, the value was estimated to be 0.21. However, this value increased to 0.41, 0.38, and 0.54 for the O_2-MWCNTs, N_2-MWCNTs and N_2+O_2-MWCNTs, respectively. The enhancement of I_D/I_G values clearly indicates the formation of more defects in the CNTs crystal structure by destruction of the C═C bonds and an increase of the sp^3 contents (keto, hydroxyl, and carboxyl groups). The I_D/I_G ratio for PAMPS-*g*-MWCNTs formed by OPIG, NPIG, and NOPIG processes were found to be 0.71, 0.67, and 0.87, respectively. Moreover, both the G and D bands shifted to the higher wavenumbers (called blue shift), especially the G band after being coated with the polymer layer. This blue shifting ensures the covalent attachment of PAMPS onto the surface of the MWCNTs.

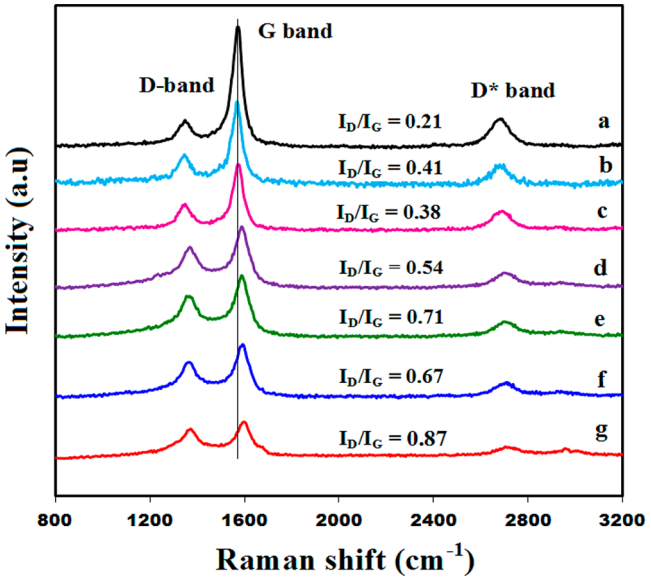

Figure 2. Raman spectra of (a) raw MWCNTs, (b) O_2-MWCNTs, (c) N_2-MWCNTs, (d) N_2+O_2-MWCNTs, (e) OPIG-PAMPS-*g*-MWCNTs, (f) NPIG-PAMPS-*g*-MWCNTs, and (g) NOPIG-PAMPS-*g*-MWCNTs.

The details of the changes in surface chemical structure of the modified MWCNTs were further ascertained by XPS study. Figure 3 compares the XPS survey spectra of raw MWCNTs,

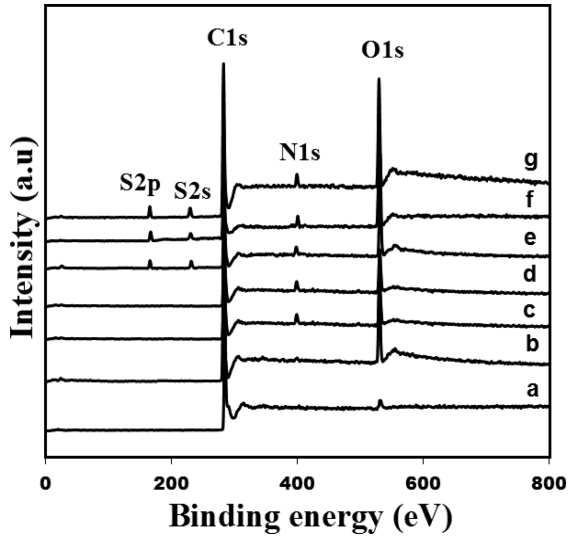

Figure 3. XPS survey spectra of (a) raw MWCNTs, (b) O_2-MWCNTs, (c) N_2-MWCNTs, (d) N_2+O_2-MWCNTs, (e) OPIG-PAMPS-*g*-MWCNTs, (f) NPIG-PAMPS-*g*-MWCNTs, and (g) NOPIG-PAMPS-*g*-MWCNTs.

O_2-MWCNTs, N_2-MWCNTs, N_2+O_2-MWCNTs, and their corresponding PAMPS-*g*-MWCNTs samples. The XPS spectrum of the raw MWCNTs (Figure 3a) had a strong peak at 284.8 eV and a small peak at 532 eV, assigned to C1s and O1s (may be due to oxidation or contamination of the raw MWCNTs), respectively. Although, after plasma treatments, the height of the O1s peaks (Figure 3b–d) increased significantly, indicating a higher concentration of oxygen introduced on the surface of CNTs during the mechanism. In case of N_2-MWCNTs and N_2+O_2-MWCNTs, a clear N1s peak

dx.doi.org/10.1021/am404768v | ACS Appl. Mater. Interfaces 2014, 6, 664–670

was detected at 400 eV, which corresponds to the presence of nitrogenated functional groups on the nanotubes surfaces too. The detailed elemental analysis (Table 1) showed that N_2+O_2-MWCNTs contained 16.88% of atomic oxygen (O/C = 0.22) and 4.67% (N/C = 0.06) atomic nitrogen on its surfaces, the sum of which is even higher than the amount of oxygen and nitrogen atoms in the O_2-MWCNTs and N_2-MWCNTs themselves. It can also be seen from Table 1 data that that the graphitic-like carbon component (sp^2 C═C) decreased greatly after the plasma treatment whereas the sp^3-hybridized carbon (C—C) as well as the C—O/C—N, C═O, and O—C═O/N—C═O components increased significantly. This clearly suggests that the surface oxidation of MWCNTs by plasma treatments took place at the expense of C═C bonds. In case of PAMPS-*g*-MWCNTs (Figure 3e−g) samples, the appearances of new peaks at 399 (N1s), 230 (S2s), and 168 eV (S2p) attributed to the successful grafting of PAMPS onto the surface of MWCNTs. Nevertheless, the highest intensity of O1s and N1s peaks was observed for the NOPIG-PAMPS-*g*-MWCNTs (Figure 3g), and is in good agreement with the results of FTIR. From Table 1, it can also be seen that NOPIG-PAMPS-*g*-MWCNTs had the highest percentages among the three PAMPS-*g*-MWCNT samples, i.e., 24.97%, 5.55%, and 5.66% in atomic oxygen, nitrogen, and sulfur, respectively. These results clearly demonstrate that NOPIG is a more effective method toward a higher degree of surface grafting to the MWCNTs as compared to the OPIG and NPIG grafting methods.

The C1s, O1s, and N1s core level spectra for the raw MWCNT and various grafted MWCNTs are presented in Figure 4. Deconvolution of the C1s peak of the raw MWCNTs (Figure 4i) at 284.6 eV (C1) was attributed to the graphitic structure (C═C).[26] The peak that appeared at 285.4 eV (C2) was related to sp^3-hybridized carbon atoms (C—C).[26] Peaks at 286.4 (C3), 287.4 (C4), and 288.8 eV (C5) correspond to C atoms attached to different oxygen containing components such as alcohols, ethers, ketones, aldehydes, esters, carboxylic acid, etc.[26,42,43] The last peak at 291.1 eV (C6) was assigned to the $\pi-\pi$ transition levels.[26,42] Figure 4iv,vii,x demonstrates the high resolution XPS C1s spectra of the PAMPS-*g*-MWCNTs prepared by OPIG, NPIG, and NOPIG, respectively. As can be seen, after grafting irrespective of the processes, the intensity of the hydrophilic groups (C3, C4, and C5) was higher than the raw MWCNTs and the width of the peaks were even broader. It can also be shown from Figure 4ii that the O1s peak for the raw MWCNTs is very weak and deconvolved into two peaks, whereas all the PAMPS-*g*-MWCNTs samples had three deconvoluted O1s peaks (Figure 4v,viii,xi). The peaks at 531.8, 532.9, and 534.3 eV were attributed to the hydroxyl, ketone, and carboxyl/sulfonic groups, respectively. The N1s spectra for the PAMPS-*g*-MWCNTs are shown in Figure 4vi,ix,xii, correspondingly. The peak fitting of N1s results showed two components at a binding energy of 399.7 and 401.8 eV, corresponding to the C—N and N—C═O functional groups[43,44] generated from PAMPS. However, the relative intensity of the O1s and N1s peaks were found to be much stronger in NOPIG-PAMPS-*g*-MWCNTs than that of the other two grafted MWCNTs, suggesting more profound grafting of PAMPS on the surface of MWCNTs by the N_2 + O_2 plasma treatment process. It must be noted that even if we increase the exposure time for O_2 and N_2 plasma processes, they cannot compete with the NOPIG process, and thus a significant difference in the grafting values was noticed. The

Table 1. XPS Results of the Deconvoluted C1s Peak and Atomic Concentrations of MWCNTs before and after Surface Modification

	concentrations of chemical species (%)						element ratio			
samples	(C1) 284.6 eV −C═C	(C2)285.4 eV −C—C	(C3)286.4 eV −C—O/C—N	(C4)287.4 eV −C═O	(C5)288.8 eV O—C═O/N—C═O	(C6) 291.1 eV $\pi-\pi^*$	C	O	N	S	O/C
raw MWCNTs	76.41 (±3.1)	8.0 (±2.0)	4.76 (±0.9)	3.64 (±0.6)	3.49 (±0.5)	3.70 (±0.5)	96.87 (±0.4)	3.13 (±0.3)			0.03
O_2-MWCNTs	54.86 (±2.8)	16.23 (±2.1)	12.16 (±1.8)	7.72 (±1.3)	5.86 (±1.0)	3.17 (±0.6)	81.45 (±0.7)	18.55 (±0.5)			0.23
N_2-MWCNTs	60.26 (±2.7)	12.04 (±1.8)	9.98 (±1.3)	6.88 (±1.2)	5.57 (±1.3)	5.27 (±0.8)	82.55 (±0.9)	12.61 (±0.7)	4.84 (±0.3)		0.15
(N_2+O_2)-MWCNTs	53.22 (±2.5)	16.94 (±1.7)	12.61 (±1.3)	7.99 (±1.1)	6.12 (±0.7)	3.12 (±0.7)	78.45 (±0.5)	16.88 (±0.5)	4.67 (±0.4)		0.22
OPIG -PAMPS-*g*-MWCNTs	47.0 (±2.2)	23.40 (±1.9)	13.25 (±1.6)	8.70 (±1.5)	5.58 (±0.5)	2.07 (±0.2)	67.77 (±1.8)	22.17 (±1.3)	4.88 (±0.7)	5.18 (±0.5)	0.33
NPIG-PAMPS-*g*-MWCNTs	47.87 (±1.7)	23.02 (±1.6)	12.50 (±1.0)	8.55 (±1.4)	5.59 (±1.0)	2.47 (±0.4)	69.76 (±2.0)	20.54 (±1.4)	4.70 (±0.6)	5.0 (±0.4)	0.29
NOPIG-PAMPS-*g*-MWCNTs	39.83 (±1.9)	24.66 (±1.5)	15.53 (±1.1)	10.65 (±0.9)	7.23 (±0.8)	2.10 (±0.4)	63.82 (±1.5)	24.97 (±0.9)	5.55 (±0.5)	5.66 (±0.4)	0.39

dx.doi.org/10.1021/am404768v | ACS Appl. Mater. Interfaces 2014, 6, 664−670

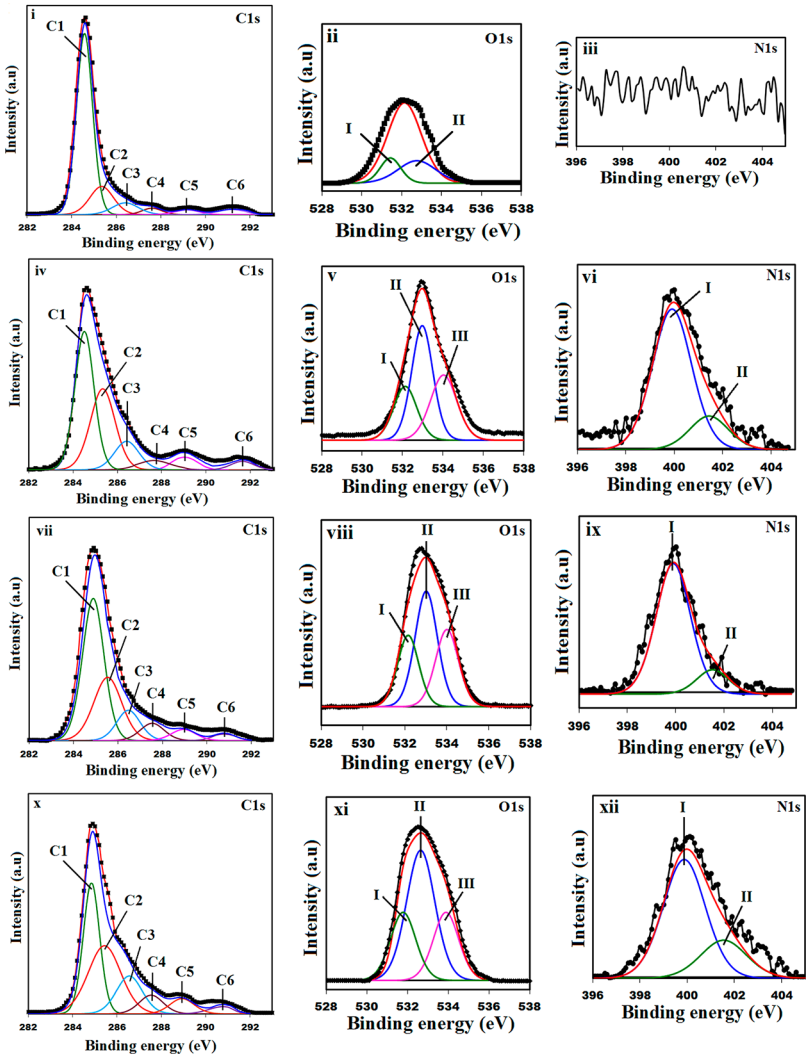

Figure 4. High resolution C1s, O1s, and N1s XPS spectra of (i–iii) raw MWCNTs, (iv–vi) OPIG-PAMPS-*g*-MWCNTs, (vii–ix) NPIG-PAMPS-*g*-MWCNTs, and (x–xii) NOPIG-PAMPS-*g*-MWCNTs.

NOPIG process is furnished with a mixture of two high polar gasses, i.e., O_2 and N_2, which provides more effective and vigorous surface treatments than that of individual OPIG and NPIG, which contain only one type of gas.

Figure 5 shows the TGA thermograms of the various PAMPS-*g*-MWCNTs. As can be seen from Figure 5a, the raw MWCNTs are very stable and do not show any significant decomposition in the temperature range 30–750 °C. The slight decomposition between 300–800 °C may be due to the presence of functional groups (formed during purification) or moisture present in the tubes. On the other hand, the polymer grafted MWCNTs (Figure 5b–d) exhibited less thermal stability and rapid mass loss profiles by multiple decomposition stages at low temperature. These can be attributed due to the weight loss of absorbed water, decomposition of surface grafted PAMPS, and some residual oxygenated and nitrogenated groups that did not react with AMPS. It is also apparent that compared to OPIG-*g*-MWCNTs (Figure 5b) and NPIG-*g*-MWCNTs (Figure 5c) samples, the weight loss is faster and more prominent for NOPIG-*g*-MWCNTs (Figure 5d), indicating a higher amount of polymer grafting on its surfaces. This once again confirmed that the mixture of nitrogen and oxygen gas plasma treatment is a highly effective method in the surface oxidation of MWCNTs. The DTG curve of NOPIG-PGMA-*g*-MWCNTs shows a higher value of peak temperature of thermal degradation at around 308 °C. According to the TGA curves, the weight percentage of grafted PAMPS on the surface of MWCNTs was estimated to be 80%, 74%, and 71% for the NOPIG-PAMPS-*g*-MWCNTs, OPIG-PAMPS-*g*-MWCNTs, and NPIG-PAMPS-*g*-MWCNTs, respectively.

The presence of a grafted polymer on the surface of MWCNTs can be visualized through HR-TEM analysis. Figure 6a–d shows the TEM images of the raw OPIG-PAMPS-*g*-MWCNTs, NPIG-PAMPS-*g*-MWCNTs, and NOPIG-PAMPS-*g*-MWCNTs, respectively. It can be seen that the surface of raw MWCNTs is smooth and tidy (Figure 6a) due to the perfect lattice structure. In contrast, the polymer coated MWCNTs showed some roughness on the surfaces, caused by the grafting of polymer chains, which can be seen clearly in Figure 6b–d. The average thickness of the encapsulated polymer layers was found to be approximately 5–7, 4–6, and 8–11 nm for OPIG, NPIG, and NOPIG processes, respectively. These variations in polymer thickness for the above mentioned processes can be explained due to the uneven surface defects that occurred, which in turn act as nucleating sites for the polymerization of AMPS molecules during different ways of grafting treatments.

dx.doi.org/10.1021/am404768v | *ACS Appl. Mater. Interfaces* 2014, 6, 664–670

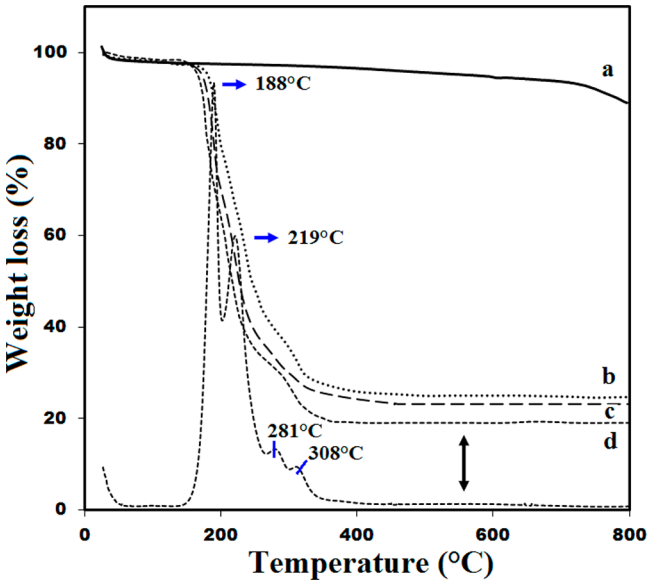

Figure 5. TGA thermograms of (a) raw MWCNTs, (b) OPIG-PAMPS-*g*-MWCNTs, (c) NPIG-PAMPS-*g*-MWCNTs, and (d) NOPIG-PAMPS-*g*-MWCNTs.

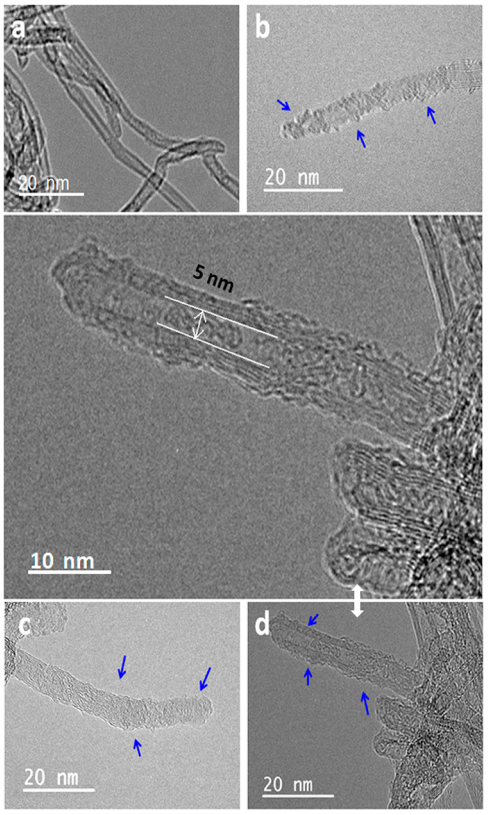

Figure 6. HRTEM images of (a) raw MWCNTs, (b) OPIG-PAMPS-*g*-MWCNTs, (c) NPIG-PAMPS-*g*-MWCNTs, and (d) NOPIG-PAMPS-*g*-MWCNTs. Arrows show the polymer layers wrapped on the nanotubes. The big image at the center shows the high magnified NOPIG-AMPS-*g*-MWCNTs for better clarity.

These results confirmed that covalent functionalization of MWCNTs by the NOPIG process is indeed a profound and efficient surface modification method.

Figure 7 shows the digital photographs of the raw and three grafted MWCNTs dispersed in methanol after being left for 30 min to 3 days at room temperature. It was observed that the raw MWCNTs aggregate and precipitate completely within 20 min after sonication, due to inert (hydrophobic) surfaces. On the other hand, when the PAMPS chains were attached to the wall of the MWCNTs, the dispersion of the PAMPS-*g*-MWCNTs (Figure 7b–d) in the methanol become extremely stable, and due to the chemical affinity between the polar groups and the organic solvent, the resulting solutions remained black suspensions even after 3 days. However, within the three grafted MWCNTs, it can be noticed even with unaided eyes that NOPIG-PAMPS-*g*-MWCNTs sustained the dispersion stability much higher. On the basis of the above findings, it can be inferred that a combination of oxygen and nitrogen functional groups present on the modified carbon nanotubes renders better surface grafting and dispersibility than that of oxygenated or nitrogenated functional groups individually. This may be due to the combined effects of the two polar and more reactive gasses that render more aggressive surface oxidation property than the individual ones.

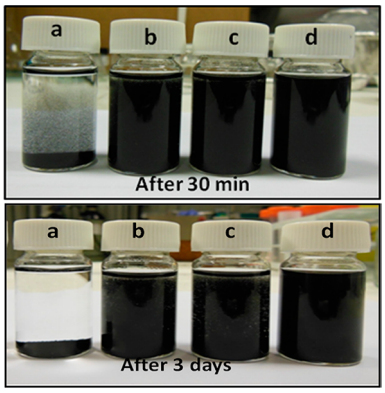

Figure 7. Digital photographs of (a) raw MWCNTs, (b) NPIG-PAMPS-*g*-MWCNTs, (c) OPIG-PAMPS-*g*-MWCNTs, (d) and NOPIG-PAMPS-*g*-MWCNTs after dispersion in methanol.

CONCLUSIONS

In summary, we have demonstrated a facile and effective method for the grafting of MWCNTs with PAMPS via a comparative study between oxygen plasma induced grafting (OPIG), nitrogen plasma induced grafting (NPIG), and nitrogen + oxygen plasma induced grafting (NOPIG) techniques. FTIR, XPS, and Raman data proved that the surface grafting of MWCNTs was successful. However, of the three grafting techniques studied, the NOPIG executed better polymer grafting and higher functionalities. The TEM images showed that all the grafted MWCNTs were covered by a thick layer of polymer around the surface. Nevertheless, thicker and uniform polymer layers were found on the NOPIG-PAMPS-*g*-MWCNTs. These results demonstrated that a mixture of nitrogen and oxygen plasma induced grafting is a very effective technique for improving the grafting degree and dispersion stability of CNTs. Using this methodology, a large variation of monomers can be covalently attached onto the CNTs surface with higher grafting degree. Also, due to simple, convenient, and inexpensive processes, we believe that this approach can be utilized for mass production of polymer encapsulated CNTs and can find applications in diverse biological and other industrial fields.

dx.doi.org/10.1021/am404768v | *ACS Appl. Mater. Interfaces* 2014, 6, 664–670

AUTHOR INFORMATION

Corresponding Authors

*C. Y. Yue. E-mail: mcyyue@ntu.edu.sg. Fax: +65-6792-4062. Tel: +65-6790-6490.

*X. Hu. E-mail: asxhu@ntu.edu.sg. Fax: +65-6790-9081. Tel: +65-6790-4610.

Notes

The authors declare no competing financial interest.

ACKNOWLEDGMENTS

The authors acknowledge the financial support of MIMO thematic program A-Star through Nanyang Technological University, Singapore.

REFERENCES

(1) Iijima, S. *Nature* **1991**, *354*, 56−58.

(2) Ren, S.; Bernardi, M.; Lunt, R. R.; Bulovic, V.; Grossman, J. C.; Gradečak, S. *Nano Lett.* **2011**, *11*, 5316−5321.

(3) Bachtold, A.; Hadley, P.; Nakanishi, T.; Dekker, C. *Science* **2001**, *294*, 1317−1320.

(4) Kasumov, A.; Deblock, R.; Kociak, M.; Reulet, B.; Bouchiat, H.; Khodos, I.; Gorbatov, Y. B.; Volkov, V. T.; Journet, C.; Burghard, M. *Science* **1999**, *284*, 1508−1511.

(5) Shin, W. H.; Jeong, H. M.; Kim, B. G.; Kang, J. K.; Choi, J. W. *Nano Lett.* **2012**, *12*, 2283−2288.

(6) Landi, B. J.; Ganter, M. J.; Cress, C. D.; DiLeo, R. A.; Raffaelle, R. P. *Energy Environ. Sci.* **2009**, *2*, 638−654.

(7) Sivakkumar, S. R.; MacFarlane, D. R.; Forsyth, M.; Kim, D. W. *J. Electrochem. Soc.* **2007**, *154*, A834−A338.

(8) Niu, C.; Sichel, E.; Hoch, R.; Moy, D.; Tennet, H. *Appl. Phys. Lett.* **1997**, *70*, 1480−1482.

(9) Popov, V. N. *Mater. Sci. Eng., R* **2004**, *43*, 61−102.

(10) Zhang, C.; Tjiu, W. W.; Liu, T.; Lui, W. Y.; Phang, I. Y.; Zhang, W. D. *J. Phys. Chem. B* **2011**, *115*, 3392−3399.

(11) Che, G.; Lakshmi, B. B.; Fisher, E. R.; Martin, C. R. *Nature* **1998**, *393*, 346−349.

(12) Cadek, M.; Coleman, J. N.; Ryan, K. P.; Nicolosi, V.; Bister, G.; Fonseca, A.; Nagy, J. B.; Szostak, K.; Béguin, F.; Blau, W. J. *Nano Lett.* **2004**, *4*, 353−356.

(13) Biercuk, M. J.; Llaguno, M. C.; Radosavljevic, M.; Hyun, J. K.; Johnson, A. T.; Fischer, J.E. *Appl. Phys. Lett.* **2002**, *80*, 2767−2769.

(14) Ajayan, P. M.; Schadler, L. S.; Giannaris, C.; Rubio, A. *AdV. Mater.* **2000**, *12*, 750−753.

(15) Yang, W.; Thordarson, P.; Gooding, J. J.; Ringer, S. P.; Braet, F. *Nanotechnology* **2007**, *18*, 412001.

(16) Gallo, M.; Favila, A.; Mitnik, D. G. *Chem. Phys. Lett.* **2007**, *447*, 105−109.

(17) Feng, Y.; Zhang, H.; Hou, Y.; McNicholas, T. P.; Yuan, D.; Yang, S.; Ding, L.; Feng, W.; Liu, J. *ACS Nano* **2008**, *2*, 1634−1638.

(18) Shin, Y. R.; Jeon, I. Y.; Baek, J. B. *Carbon* **2012**, *50*, 1465−1476.

(19) Salzmann, C. G.; Llewellyn, S. A.; Tobias, G.; Ward, M. A. H.; Huh, Y.; Green, M. L. H. *Adv. Mater.* **2007**, *19*, 883−887.

(20) Liu, P. *Eur. Polym. J.* **2005**, *41*, 2693−2703.

(21) Plank, N. O. V.; Jiang, L.; Cheung, R. *Appl. Phys. Lett.* **2003**, *83*, 2426.

(22) Lin, C. C.; Huang, H. C. *J. Power Sources* **2009**, *188*, 332−337.

(23) Meng, F. Y.; Ogata, S.; Xu, D. S.; Shibutani, Y.; Shi, S. Q. *Phys. Rev. B: Condens. Matter Mater. Phys.* **2007**, *75*, 205403.

(24) Felten, A.; Bittencourt, C.; Pireaux, J. J.; Lier, G.V.; Charlier, J.C. *J. Appl. Phys.* **2005**, *98*, 074308.

(25) Bertóti, I.; Mohai, I.; Mohai, M.; Szépvölgyi, J. *Diamond Relat. Mater.* **2011**, *20*, 965−968.

(26) Zhao, B.; Zhang, L.; Wang, X.; Yang, J. *Carbon* **2012**, *50*, 2710−2716.

(27) Szetsen, L.; Peng, Jr-W. *J. Phys. Chem. Solids* **2011**, *72*, 1101−1103.

(28) Xu, L.; Fang, Z.; Song, P.; Peng, M. *Plasma Process Polym.* **2010**, *7*, 785−793.

(29) Petrov, P.; Georgiev, G.; Momekova, D.; Momekov, G.; Tsvetanov, C. B. *Polymer* **2010**, *51*, 2465−2471.

(30) Zhang, H.; Guo, H.; Deng, X.; Gu, P.; Chen, Z.; Jiao, Z. *Nanotechnology* **2010**, *21*, 085706.

(31) Zhao, B.; Hu, H.; Haddon, R. C. *Adv. Funct. Mater.* **2004**, *14*, 71−76.

(32) Huang, Y. L.; Ma, C. H. M.; Yuen, S. M.; Chuang, C. Y.; Kuan, H. C.; Chiang, C. L.; Wu, S. Y. *Mater. Chem. Phys.* **2011**, *129*, 1214−1220.

(33) Chen, S.; Wu, G.; Liu, Y.; Long, D. *Macromolecules* **2006**, *39*, 330−334.

(34) Qin, S.; Qin, D.; Ford, W. T.; Herrera, J. E.; Resasco, D. E.; Bachilo, S. M.; Weisman, R. B. *Macromolecules* **2004**, *37*, 3965−3967.

(35) Yao, Z.; Braidy, N.; Botton, G. A.; Adronov, A. *J. Am. Chem. Soc.* **2003**, *125*, 16015−16024.

(36) Sakellariou, G.; Ji, H.; Mays, J. W.; Baskaran, D. *Chem. Mater.* **2008**, *20*, 6217−6230.

(37) Lee, R. H.; Chen, W. H.; Lin, J. H. *Polymer* **2011**, *52*, 2180−2188.

(38) Roy, S.; Yue, C. Y.; Lam, Y. C.; Wang, Z. Y.; Hu, H. *Sens. Actuators, B* **2010**, *150*, 537−549.

(39) Kuroki, H.; Ohashi, H.; Ito, T.; Tamaki, T.; Yamaguchi, T. *J. Membr. Sci.* **2010**, *352*, 22−31.

(40) Limparyoon, N.; Seetapan, N.; Kiatkamjornwong, S. *Polym. Degrad. Stab.* **2011**, *96*, 1054−1063.

(41) Schroeder, M.; Fatarella, E.; Kovac, J.; Guebitz, G. M.; Kokol, V. *Biomacromolecules* **2008**, *9*, 2735−2741.

(42) Datsyuk, V.; Kalyva, M.; Papagelis, K.; Parthenios, J.; Tasis, D.; Siokou, A.; Kallitsis, I.; Galiotis, C. *Carbon* **2008**, *46*, 833−840.

(43) Roy, S.; Yue, C. Y.; Venkatraman, S. S.; Ma, L. L. *J. Mater. Chem.* **2011**, *21*, 15031−15040.

(44) Abbas, A.; Vercaigne, D. M.; Supiot, P.; Bocquet, B.; Vivien, C.; Guillochon, D. *Colloids Surf., B* **2009**, *73*, 315−324.